JACC Vol. 30, No. 7
December 1997:1892–9

Three-Dimensional Myocardial Contrast Echocardiography: Validation of In Vivo Risk and Infarct Volumes

ANDRE Z. LINKA, MD, GURSEL ATES, MD, KEVIN WEI, MD, SOROOSH FIROOZAN, MD, DANNY M. SKYBA, PHD, SANJIV KAUL, MD, FACC

Charlottesville, Virginia

Objectives. **The aim of this study was to determine whether three-dimensional (3D) myocardial contrast echocardiography (MCE) could provide an accurate in vivo assessment of risk and infarct volumes.**

Background. **MCE has been shown to accurately define risk area and infarct size in single tomographic slices. The ability of this technique to measure risk and infarct volumes by using three-dimensional echocardiography (3DE) has not been determined.**

Methods. **Fifteen open chest dogs underwent variable durations of coronary artery occlusion followed by reperfusion. At each stage, MCE was performed by using left atrial injection of AIP201, a deposit microbubble with a mean diameter of 10 ± 4 μm and a mean concentration of $1.5 \cdot 10^7 \cdot ml^{-1}$. Images were obtained over a 180° arc with use of an automated rotational device and were stored in computer as a 3D data set. Postmortem risk area and infarct size were measured in six to eight left ventricular short-axis slices of equal thickness using technetium-99m autoradiography and tissue staining, respectively. MCE images corresponding to these planes were reconstructed off-line.**

Results. **A close linear relation was noted between the volume of myocardium not showing contrast enhancement on 3D MCE during coronary occlusion and postmortem risk volume ($y = 1.2x - 3.0$, $r = 0.83$, SEE = 5.1, $n = 15$). The volume of myocardium not showing contrast enhancement on 3D MCE after reperfusion also closely correlated with postmortem infarct volume ($y = 1.1x - 3.9$, $r = 0.88$, SEE = 4.8, $n = 11$). No changes in systemic hemodynamic variables were noted with injections of AIP201.**

Conclusions. **When combined with AIP201, a deposit microbubble, 3D MCE can be used to accurately determine both risk and infarct volumes in vivo. This method could be used to assess the effects of interventions that attempt to alter the infarct/risk volume ratio.**

(J Am Coll Cardiol 1997;30:1892–9)

Myocardial contrast echocardiography (MCE) has been shown to reliably estimate risk area during coronary occlusion in several studies (1–8). However, these studies were performed by using a single tomographic plane, which does not provide an accurate assessment of the entire left ventricular (LV) risk volume. Similarly, MCE has been demonstrated to accurately define infarct size after reperfusion (5–11) by using the principle that micro-vascular damage occurs within the infarction (12–14). Again, single tomographic planes were used, which do not necessarily reflect the size or topography of the total LV infarct volume. Most microbubbles used in MCE behave like red blood cells when injected arterially, and they clear the myocardium very shortly after an arterial injection. Therefore, to obtain an assessment of the three-dimensional (3D) topography of risk and infarct volumes during arterial injections of these microbubbles, several injections and images from multiple views are required (3). Use of a single injection of a safe deposit tracer would make the acquisition of the 3D data set more convenient. We postulated that combining 3D MCE with a stable deposit microbubble would provide accurate information on risk volume during coronary artery occlusion and infarct volume after reperfusion. We also assessed the effects of this new deposit microbubble on cardiac and systemic hemodynamics.

Methods

Animal preparation. The study protocol was approved by the Animal Research Committee at the University of Virginia

From the Cardiovascular Division, University of Virginia, Charlottesville, Virginia. This study was supported in part by grants from the National Heart, Lung, and Blood Institute, National Institutes of Health (RO1-HL48890), Bethesda, Maryland and Andaris Ltd., Nottingham, England, United Kingdom and an equipment grant from Advanced Technology Laboratories, Bothell, Washington. Dr. Linka was supported by the Ciba-Geigy Jubiläums-Stiftung, Basel, Switzerland and the Theodor und Ida Herzog-Egli Stiftung, Zürich, Switzerland. Dr. Ates was the recipient of a grant from the Turkish Cardiology Society, Istanbul, and Dr. Firoozan was the recipient of a Junior Research Fellowship from the British Heart Foundation, London, England, United Kingdom. Dr. Wei was the recipient of a Junior Personnel Research Fellowship from the Heart and Stroke Foundation of Canada, Ottawa, Ontario, Canada, and Dr. Skyba is the recipient of a postdoctoral fellowship grant (F32-HL-09540) from the National Institutes of Health. Dr. Kaul was an Established Investigator of the American Heart Association, Dallas, Texas. This work was presented in part at the 7th Annual Scientific Session of the American Society of Echocardiography, Orlando, Florida, June 1997.

Manuscript received May 14, 1997; revised manuscript received August 15, 1997, accepted August 21, 1997.

Address for correspondence: Dr. Sanjiv Kaul, Cardiovascular Division, Box 158, University of Virginia, Medical Center, Charlottesville, Virginia 22908. E-mail: sk@virginia.edu.

0735-1097/97/$17.00
PII S0735-1097(97)00359-8

Abbreviations and Acronyms

ANOVA = analysis of variance
LAD = left anterior descending coronary artery
LCx = left circumflex coronary artery
LV = left ventricular
LV dP/dt = first derivative of left ventricular pressure
MCE = myocardial contrast echocardiography (echocardiographic)
Tc-99m = technetium-99m
3D = three-dimensional
3DE = three-dimensional echocardiography (echocardiographic)
VI = video intensity

and conformed to the American Heart Association "Guidelines for Use of Animals in Research." Fifteen adult mongrel dogs weighing 26 to 34 kg (median 31) were anesthetized with 30 mg·kg^{-1} of sodium pentobarbital (Abbott Laboratories). They were intubated, and ventilated with room air by means of a respirator pump (model 607, Harvard Apparatus) with use of a positive end-expiratory pressure of 3 to 5 cm H_2O. Additional anesthetic agents were administered during the experiment as needed. A 7F catheter was placed in the femoral artery and was connected by means of a fluid-filled transducer (model 1280C, Hewlett-Packard) to a multichannel recorder (model 4568C, Hewlett-Packard) for arterial pressure monitoring. Two 7F catheters were also placed in the femoral veins for intravenous administration of fluids (Plasma-Lyte A, Baxter Healthcare Corp.) and drugs. Electrocardiographic leads were attached in standard fashion.

A left lateral thoracotomy was performed and the heart was suspended in a pericardial cradle. The proximal portions of the left anterior descending (LAD) and left circumflex (LCx) coronary arteries were dissected free from the surrounding tissue, and umbilical tape was placed loosely around one of them. A 7F catheter was placed in the left atrium for pressure measurement, as well as for injections of microbubbles and technetium-99m (Tc-99m)-labeled microalbumin aggregates. The external jugular vein was cannulated with a 7F pulmonary artery balloon-tipped flotation catheter (model MPA-372T, Millar Instruments), whose tip was positioned in the proximal pulmonary artery and connected to a cardiac output computer (model 9520A, Edwards Laboratories). A micromanometer-tipped catheter (model PSPC-471A, Millar Instruments) was introduced through the left carotid artery into the left ventricle for measurement of LV pressure and its first derivative (LV dP/dt). Arterial blood gases were monitored throughout each experiment (model M238, Ciba Corning, Essex, England, United Kingdom) and kept at physiologic levels.

Hemodynamic measurements. Arterial, LV, pulmonary artery and left atrial pressures and LV dP/dt were monitored continuously throughout the experiment. The multichannel recorder was interfaced with a 386-based personal computer by way of an eight-channel analog to digital converter (DAS-16, Metrabyte). Measurements were made at baseline as well as during coronary occlusion and reperfusion, before and repeatedly after contrast injection. Data were sampled at 200 Hz with use of Labtech Notebook (Laboratory Technologies Corp.). Cardiac output (an average of three measurements) was also recorded immediately before and after each contrast injection.

MCE. AIP201 (Andaris Ltd., Nottingham, England, United Kingdom) was used as the contrast agent. This agent is formed by spraying 5% human albumin solutions, which form air-filled bubbles with 1-μm thick denatured albumin shells. The mean size of the bubbles is 10 ± 4 μm (90% >7 μm and 0.5% ≥20 μm) and the mean concentration is $1.5 \cdot 10^7 \cdot ml^{-1}$. It is delivered as a white powder that is reconstituted with 5 ml of 10 $\mu g \cdot ml^{-1}$ of Tween-80. In pilot series, a dose of 10 to 15 ml (0.3 to 0.5 $ml \cdot kg^{-1}$) was found to provide optimal myocardial opacification without system saturation or attenuation.

MCE was performed by using a phased array system (HDI 3000cv, Advanced Technology Laboratories) capable of both fundamental imaging (ultrasound transmitted and received at 3 MHz) and harmonic imaging (ultrasound transmitted at 2.3 MHz and received at 4.6 MHz). A dynamic range of 60 dB, a frame rate of 30 Hz and a mechanical index of 0.7 to 0.9 were used. Images were recorded on 1.25-cm S-VHS videotape (Panasonic AG-MD830, Matsushita Electric). A saline bath acted as an acoustic interface between the heart and the transducer.

MCE images for 3D reconstruction were acquired as previously described (15). The transducer was mounted in a rubber housing and attached to a rotational device (TomTec), which in turn was attached to a steel arm that was fixed above the saline bath to ensure a stable position. The video output of the ultrasound machine was connected to a 3D echocardiographic (3DE) reconstruction system resident on a personal computer (TomTec, Echo-Scan 3.0). Imaging was performed by automatically rotating the transducer clockwise at 2° increments over a 180° arc. To achieve optimal spatial and temporal data registration, system-based algorithms were used to ensure that data acquisition occured at a predefined RR interval during end-expiration. The 90 end-diastolic cross sections sampled in this manner were digitized and stored in computer memory.

The images were converted off-line from a polar to a Cartesian coordinate system in a 256 × 256 × 256 pixel format with 8-bit pixel resolution. Mathematic interpolation and standard smoothing algorithms were applied to reduce noise and spatial artifacts. Optimal long- and short-axis views were reconstructed from the 3D data with a slice thickness of 0.5 cm. The perfusion defects during coronary occlusion and reperfusion were planimetered at each short-axis level. The areas of these individual slices were summed and multiplied by the sum of the distance between adjacent planes (0.5 cm) to obtain the total risk and infarct volumes.

Technetium autoradiography. A median of 33 min before reperfusion, 20 to 30 mCi of 20- to 40-μm Tc-99m–labeled microalbumin aggregates (Macrotec, Bracco Diagnostics Inc.) were injected into the left atrium for autoradiography (16). A clear plastic sheet was placed over the postmortem heart slices (see later), and the epicardial and endocardial (excluding the

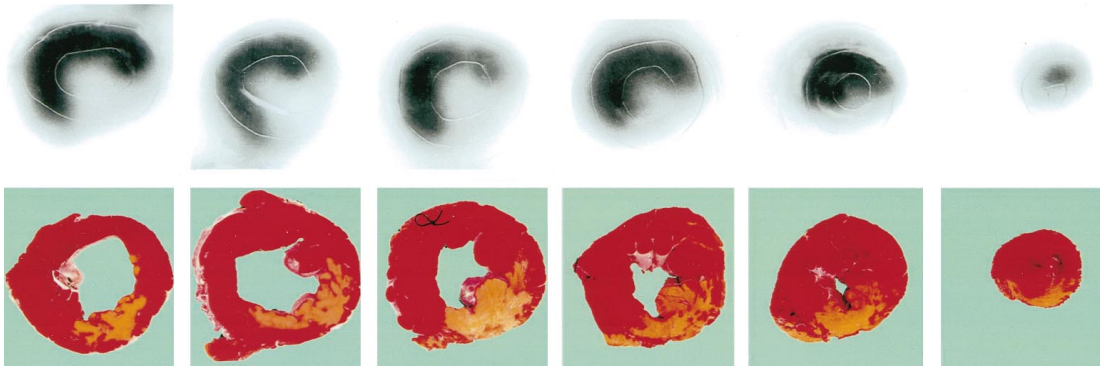

Figure 1. Tc-99m autoradiography (**top row**) and postmortem infarct staining (**bottom row**) in the same heart as an example of LCx occlusion and reperfusion. Because Tc-99m was injected during coronary occlusion, all the areas with blood flow are shown in **black,** whereas the risk area is depicted by the **cold spots.** On the tissue-stained slices (**bottom row**), viable myocardium is stained **brick red** whereas the infarct bed shows no staining.

papillary muscles) contours were manually drawn over the sheet. The slices were then placed on double-emulsion X-ray film (X-Omat AR, Eastman Kodak), which was exposed overnight and developed with an automatic processor (M35A, X-Omatic, Eastman Kodak). The risk area in each slice was seen as a cold spot on the autoradiograph (Fig. 1, top panel). The plastic sheet with the myocardial contours were placed on the autoradiographs and the risk areas outlined on it. Risk areas measured from each slice were summed and multiplied by the sum of the individual slice thicknesses to obtain risk volume.

Determination of infarct size. After Tc-99m autoradiography, the heart was immersed in a solution of 1.3% 2,3,5-triphenyltetrazolium chloride (Sigma Corp.) and 0.2 mmol/liter Sörensen's buffer (KH_2PO_4 and K_2HPO_4 in distilled water, pH 7.4) at 37°C for 20 to 30 min. With this technique, noninfarcted areas are stained brick red whereas necrosed areas remain unstained (17). The slices were arranged in the same format as during autoradiography (Fig. 1, bottom panel), and the same plastic sheet on which manual contours had been drawn previously was superimposed on these slices. The infarct areas and volume were measured and calculated with the same method used for risk areas and volume assessment.

Experimental protocol. Either the LCx (n = 7) or the LAD (n = 8) was occluded for 40 to 300 min (median 165) to cause infarctions of varying sizes. After coronary occlusion, hemodynamic data were acquired and the first dose of microbubbles was injected slowly over 3 min. Hemodynamic data acquisition was performed immediately after injection and repeated every minute for 5 min. Subsequent acquisitions were made at 15-min intervals for 1 h. Toward the end of the occlusion period, MCE was repeated and followed by the left atrial injection of Tc-99m–labeled macroalbumin aggregates. Thus, the first set of images was acquired 20 to 190 min (median 125) after bubble injection. The occlusion was then released followed by 20 to 200 min (median 90) of reperfusion. When the dog was hemodynamically stable, exogenous hyperemia was induced by an intravenous infusion of 0.4 $\mu g \cdot kg^{-1} \cdot min^{-1}$ of WRC-0470 (Discovery Therapeutics Inc.), a novel, selective, adenosine-A_{2a} receptor agonist (18). The second dose of microbubbles was then injected followed by MCE data acquisition 12 to 58 (median 33) min later. Hemodynamic data were acquired in a manner similar to the occlusion stage. In pilot studies, both fundamental and harmonic imaging were performed to determine their effects on image quality. These data were not recorded. However, in the first study dog, both forms of imaging were recorded. Because no differences were noted in the myocardial contrast effect between these two modalities, harmonic imaging alone was performed in all subsequent dogs. At the end of the experiment, the dog was killed with an overdose of pentobarbital, and the heart was removed. It was cut with a macrotome into six to eight equal short-axis slices (each 0.7 to 1.0 cm thick, depending on the dog).

Statistical methods. Correlations between MCE and postmortem data were performed by using linear regression analysis. Hemodynamic data before and after contrast injections were compared at each stage by using analysis of variance (ANOVA) with repeated measures. Myocardial video intensity (VI) data (arbitrary units, 0 to 255) were compared by using a Student paired *t* test in the one dog with both harmonic and fundamental images. A p value < 0.05 (two-sided) was considered statistically significant.

Results

Quality of myocardial opacification. Immediately after microbubble injection, contrast medium was seen in the LV cavity, but it cleared in <1 min. Subsequently, myocardial opacification was excellent and remained visually unchanged over the period of observation. Although both fundamental and harmonic imaging were performed in only one dog, the image quality was similar for both forms of imaging (Fig. 2). VI averaged from the 12, 3, 6 and 9 o'clock positions measured from images were similar in these dogs (75 vs. 78, p = 0.65).

VI was measured in the myocardium between the first and second injections over an interval of 60 to 240 min (median 180 min). There was no measurable change in VI (79 ± 18 vs.

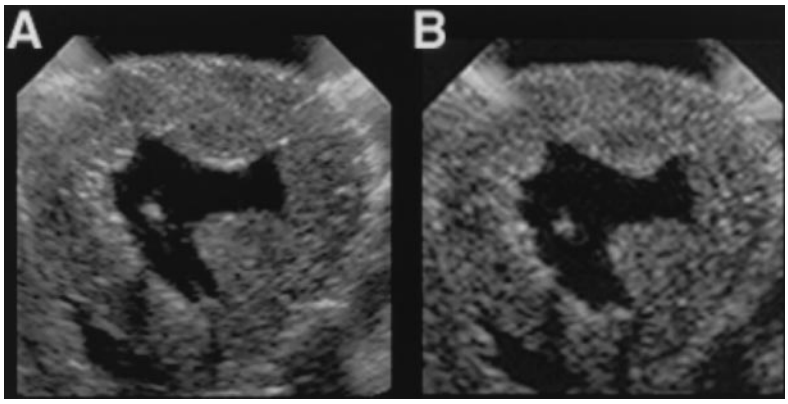

Figure 2. Examples of images obtained during fundamental **(panel A)** and harmonic **(panel B)** imaging after injection of AIP201.

78 ± 17, p = 0.32) during this period. The second injection only defined the smaller defect after reperfusion reflecting the infarct size. The larger defect from the first injection reflecting risk area was no longer seen after the second injection despite the persistence in the myocardium of microbubbles from that injection.

Validation of MCE perfusion defects. The risk area was clearly seen on MCE in all dogs during coronary occlusion. Figure 3 demonstrates the perfusion defects in several short-axis planes that were reconstructed from a 3D data set in a dog during LCx occlusion. Figure 4A depicts a close linear relation between 3D MCE perfusion defects during coronary occlusion and risk volumes derived by Tc-99m autoradiography.

After reperfusion, two dogs died before image acquisition. In two other dogs 3D images were of insufficient quality owing to electrical or hemodynamic instability. The data from the remaining 11 dogs are presented in Figure 4B. A close linear relation between 3D MCE perfusion defects during hyperemia and postmortem-defined infarct volume was noted. Figure 5 illustrates an example of a small perfusion defect after reperfusion in a dog whose infarct involved the basal portion of the LCx territory.

Hemodynamic effects. As expected, during coronary occlusion and reperfusion, all dogs experienced some hemodynamic instability. In four dogs, defibrillation was required. The injections were always performed after the dog had become hemodynamically stable. No significant differences were noted in heart rate; aortic, pulmonary artery or left atrial pressures;

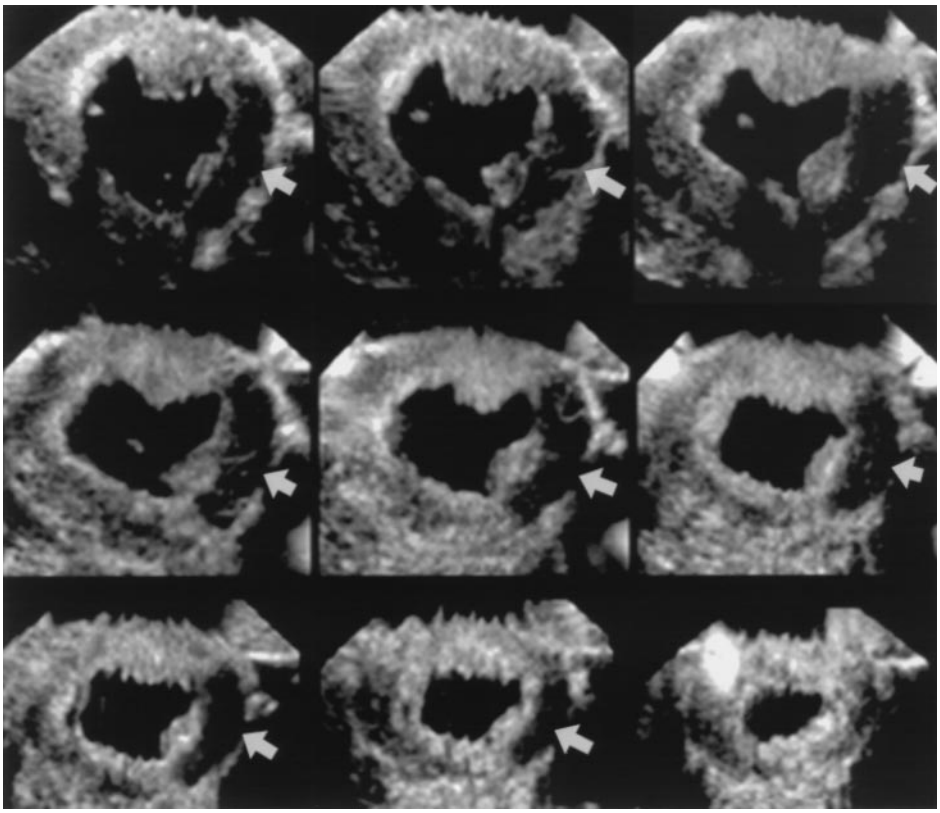

Figure 3. Reconstructed 3D MCE data set during LCx occlusion. Nine 0.5-cm thick short-axis views are displayed. The perfusion defect denoting the risk area is depicted by **arrows.**

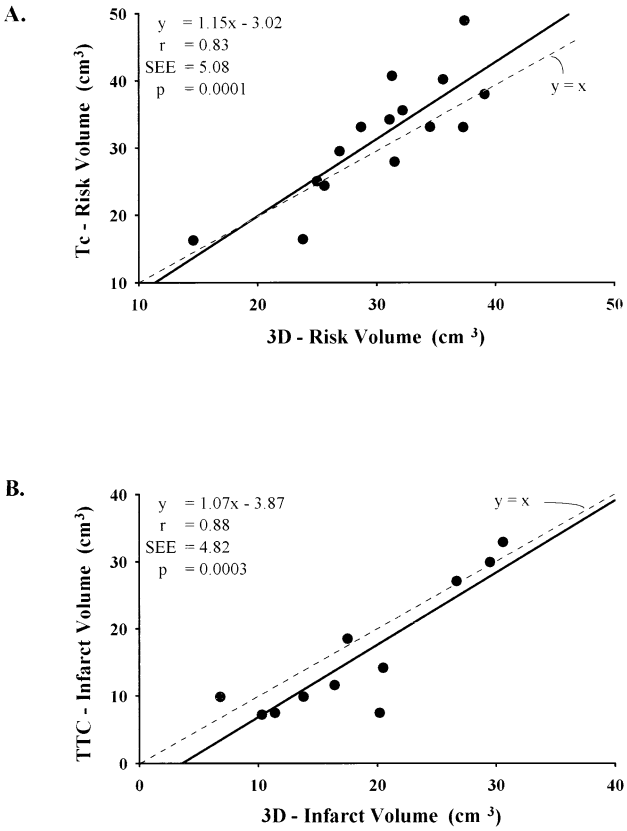

Figure 4. Relations between perfusion defect volumes obtained by 3D MCE during coronary occlusion (**A**) and reperfusion (**B**) with postmortem estimates of risk and infarct volumes, respectively. See text for details. Tc = technetium; TTC = triphenyl tetrazolium chloride.

cardiac output; or LV dP/dt for the 1-h observation period after injection of bubbles either during coronary occlusion or during reperfusion. Figure 6 depicts the hemodynamic variables for 1 h after microbubble injection when data from the first and second injections were combined.

Figure 5. Reconstructed 3D MCE data set after reperfusion in a dog with a small infarction involving the basal portion of the LCx bed. Eight 0.5-cm thick short-axis views are displayed. The infarct size is depicted by **arrows.**

Discussion

Properties of an ideal deposit tracer. For the quantification of myocardial blood flow, an ideal deposit tracer should become wholly entrapped within the myocardium after left atrial injection. The mass of the tracer entrapped in the myocardial arterioles should be proportional to the flow to that arteriole irrespective of its location within the myocardium. The concentration of the tracer in myocardial regions should thus provide an estimation of relative blood flow to these regions. It should be possible to derive absolute blood flow to myocardial regions by measuring the concentration of the tracer in an arterial blood sample collected at a known flow rate during injection of the tracer (19–21). The closest analogy to the ideal deposit tracer is provided by radiolabeled microspheres, which require postmortem tissue analysis and are thus not suitable in the clinical setting (19).

The microbubbles used in this study are not ideal deposit tracers because they vary widely in size. The smaller bubbles (<5 to 6 μm) pass through the myocardium, whereas the larger bubbles (>7 μm) are entrapped in different myocardial arterioles in proportion to their size. Nonetheless, if the microbubbles are homogeneously suspended, because the number reaching a myocardial bed (including those that are entrapped) is determined by blood flow to that region, their myocardial distribution should provide a measure of relative flow to different regions, provided ultrasound attenuation is also homogeneous across the heart.

Deposit tracers should not cause hemodynamic perturbations within the coronary microcirculation, particularly if they are to be used clinically. It has been demonstrated (21) that up to 22 million 7- to 10-μm–sized radiolabeled microspheres can be safely administered by way of the left atrium without adverse hemodynamic effects at rest. Obviously, the number of microspheres that can be administered without deleterious results will be determined by their size. If the size distribution

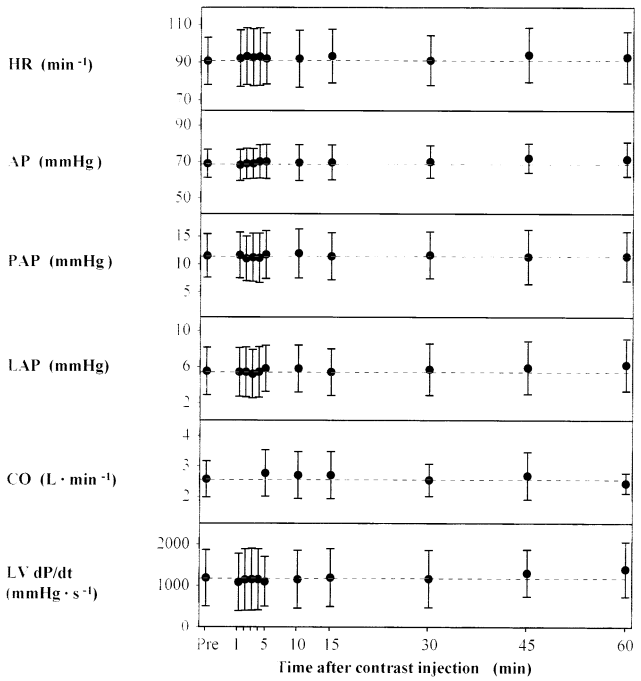

Figure 6. Hemodynamic data after contrast injection. Data from both injections are included and shown as mean value (**closed circles**) ± SEM (**bars**). AP = mean aortic pressure; CO = cardiac output; HR = heart rate; L = liters; LAP = mean left atrial pressure; PAP = mean pulmonary artery pressure; pre = before injection.

of the microbubbles entrapped within the coronary microcirculation is known, then the number of bubbles that can safely be injected can be calculated. In this study, we did not observe any hemodynamic alterations caused by the bubbles at rest for the 1-h observation period after each injection. Because ours was not a long-term study, we were not in a position to assess the long-term hemodynamic effects or safety of these microbubbles.

Deposit tracers such as Echo Gen, can also be administered intravenously provided that at the time of injection they are small enough to cross the lung capillaries, after which they expand in size, becoming trapped in the myocardial microvasculature (6). This expansion occurs when the bubbles imbibe gases (nitrogen and oxygen) present in blood. Inability to control the number and size of these larger microbubbles in vivo can result in hemodynamic perturbations due to microcirculatory blockage within the myocardium. At the dose at which Echo Gen causes optimal myocardial opacification, cardiac performance decreases even at rest (22). Importantly, at rest, the normal myocardial microvasculature has great reserve (23,24), and up to >80% of the microvasculature can be effectively blocked before hemodynamic perturbations are noted (24). In patients with ischemic heart disease, however, the point at which this reserve is exhausted varies, and the number of microbubbles that can be safely administered may be much smaller.

Unlike Echo Gen, the bubbles used in our study have a predetermined size. Because the shells of these bubbles are very thick (1 μ), gas exchange does not occur across them, and they neither enlarge nor shrink in size. The thick shells also preclude the destruction of the bubbles by ultrasound, even at high acoustic pressures. Consequently, myocardial opacification resulting from these bubbles remains unchanged for several hours even with continuous imaging. We did not observe any changes in myocardial opacification within the nonoccluded bed for several hours after left atrial injections of these bubbles.

Because AIP201 bubbles are not destroyed by ultrasound, intermittent imaging is not necessary. Nonlinear oscillation may also be minimal even at an optimal frequency because of damping caused by the thick shells. Unlike other free-flowing microbubbles, therefore, these bubbles do not require the addition of harmonic imaging to increase the signal to noise ratio. Although we used mostly harmonic imaging for our study, we found no significant differences in VI between fundamental and harmonic imaging when we used both modalities. The ability to use conventional rather than special forms of imaging may be an added advantage of these microbubbles.

Value of 3D data. Because it is a 3D structure, a single tomographic plane cannot accurately reflect pathologic involvement of the entire heart. Although multiple standard cross sections on two-dimensional echocardiography can provide an idea of the 3D topography of risk and infarct volumes, this approach has limitations. Parallel cross sections are difficult to obtain in adult patients because of the limited number of acoustic windows. Because of abnormalities in the shape of the heart afflicted with ischemic dysfunction, simple geometric models cannot be used to calculate risk and infarct volumes. These measurements can only be obtained from an actual 3D data set (25–27).

In a manner similar to that used with single-photon emission computed tomography (28), we used reconstruction to obtain the cross sections we needed. This approach is not ideal for several reasons. 1) There are many potential sources of artifacts. Differences in cardiac cycle lengths and cardiac translation caused by respiration can result in inadequate data registration. In our study, this limitation was largely overcome by selecting cycles with a predefined length and by use of respiratory gating. Despite these maneuvers, however, we could not obtain adequate data in two dogs after reperfusion because of intractable arrhythmias. 2) Any change in transducer position during image acquisition can result in data misregistration. 3) MCE images are associated with attenuation-related artifacts. As with single-photon emission computed tomography, these artifacts can be magnified by the process of reconstruction. 4) The process is tedious and time-consuming. Transducer positioning alone can take up to 30 min and image analysis can take up to several hours, depending on the quality of the images and the level of observer experience. For these reasons, this approach is unlikely to be used in the clinical setting in its present form.

A more ideal way to perform 3DE is by directly acquiring a 3D data set in a manner similar to that of magnetic resonance imaging (29). One evolving strategy is the use of an array of

arrays that can create a 3D beam wide enough to encompass the entire heart (30). Although the spatial resolution of this technique is currently not as good as that of magnetic resonance imaging, it has certain advantages. It can acquire the entire data set in one cardiac cycle, thus obviating the need for electrocardiographic or respiratory gating. It also retains the high temporal resolution of ultrasound. Unlike magnetic resonance imaging, it can also be used at the bedside. The lower equipment cost and the potentially much higher number of patients examined within a given period makes 3DE with such a system more economical and more practical than magnetic resonance imaging.

Conclusions. We have described a new deposit microbubble for MCE that produces excellent myocardial opacification after left atrial injection without causing adverse hemodynamic effects at rest at the doses used in this study. It does not require special forms of imaging, such as harmonic imaging, to obtain images with good myocardial opacification. Because of its prolonged myocardial effect, it is also ideal for 3DE. With this technique, this new agent provides accurate assessment of risk and infarct volumes. Although these data provide only proof of principle, we believe that this approach could be useful in the operating room and cardiac catheterization laboratory for assessing myocardial perfusion (31–36). In particular, it could be used to determine the effect of pharmacologic and physical interventions aimed at reducing the infarct/risk volume ratio.

We thank Norman C. Goodman, BS for technical assistance and Mr. Joseph Garzie of Advanced Technology Laboratories for assistance in data acquisition.

References

1. Tei C, Sakamaki T, Shah PM, et al. Myocardial contrast echocardiography: a reproducible technique for myocardial opacification for identifying regional perfusion deficits. Circulation 1983;67:585–93.
2. Kemper AJ, O'Boyle JE, Sharma S, et al. Hydrogen peroxide contrast-enhanced two-dimensional echocardiography: real-time in vivo delineation of regional myocardial perfusion. Circulation 1983;68:603–11.
3. Kaul S, Pandian NG, Okada RD, Pohost GM, Weyman AE. Contrast echocardiography in acute myocardial ischemia: I: in vivo determination of total left ventricular "area at risk". J Am Coll Cardiol 1984;4:1272–82.
4. Kaul S, Glasheen W, Ruddy TD, Pandian NG, Weyman AE, Okada RD. The importance of defining left ventricular area at risk in vivo during acute myocardial infarction: an experimental evaluation with myocardial contrast two-dimensional echocardiography. Circulation 1987;75:1249–60.
5. Villanueva FS, Glasheen WP, Sklenar J, Kaul S. Assessment of risk area during coronary occlusion and infarct size after reperfusion with myocardial contrast echocardiography using left and right atrial injections of contrast. Circulation 1993;88:596–604.
6. Grayburn PA, Erickson JM, Escobar J, Womack L, Velasco CE. Peripheral intravenous myocardial contrast echocardiography using a 2% dodecafluoropentane emulsion: identification of myocardial risk area and infarct size in the canine model of ischemia. J Am Coll Cardiol 1995;26:1340–7.
7. Firschke C, Lindner JR, Goodman NC, Skyba DM, Wei K, Kaul S. Myocardial contrast echocardiography in acute myocardial infarction using aortic root injections of microbubbles in conjunction with harmonic imaging: potential application in the catheterization laboratory. J Am Coll Cardiol 1997;29:207–16.
8. Firschke C, Lindner JR, Wei K, Goodman NC, Skyba DM, Kaul S. Myocardial perfusion imaging in the setting of coronary artery stenosis and acute myocardial infarction using venous injection of a second generation echocardiographic contrast agent. Circulation 1997;96:959–67.
9. Kemper AJ, O'Boyle JE, Cohen CA, Taylor A, Parisi AF. Hydrogen peroxide contrast echocardiography: quantification in vivo of myocardial risk area during coronary occlusion and of the necrotic area remaining after myocardial reperfusion. Circulation 1984;70:309–17.
10. Villanueva FS, Glasheen WP, Sklenar J, Kaul S. Characterization of spatial patterns of flow within the reperfused myocardium by myocardial contrast echocardiography: implications in determining extent of myocardial salvage. Circulation 1993;88:2596–606.
11. Villanueva FS, Camarano G, Ismail S, Goodman NC, Sklenar J, Kaul S. Coronary reserve abnormalities in the infarcted myocardium: assessment of myocardial viability immediately versus late after reflow by contrast echocardiography. Circulation 1996;94:748–54.
12. Kloner RA, Ganote CE, Jennings RB. The "no-reflow" phenomenon after temporary coronary occlusion in the dog. J Clin Invest 1974;54:1496–508.
13. Vanhaecke J, Flameng W, Borgers M, Jang IK, Van de Werf F, De Geest H. Evidence for decreased coronary flow reserve in viable postischemic myocardium. Circ Res 1990;67:1201–10.
14. Johnson WB, Malone SA, Pantely GA, Anselone CG, Bristow JD. No reflow and extent of infarction during maximal vasodilation in the porcine heart. Circulation 1988;78:462–72.
15. Nosir YFM, Fioretti PM, Vletter WB, et al. Accurate measurement of left ventricular ejection fraction by three-dimensional echocardiography—a comparison with radionuclide angiography. Circulation 1996;94:460–6.
16. DeBoer LW, Strauss HW, Kloner RA, et al. Autoradiographic method for measuring the ischemic myocardium at risk: effects of verapamil on infarct size after experimental coronary artery occlusion. Proc Natl Acad Sci U S A 1980;77:6119–23.
17. Fishbein MC, Meerbaum S, Rit J, et al. Early phase acute myocardial infarct size quantification: validation of the triphenyl tetrazolium chloride tissue enzyme staining technique. Am Heart J 1981;101:593–600.
18. Glover DK, Ruiz M, Yang JY, et al. Pharmacologic stress thallium scintigraphy with 2-cyclohexylmethylidene hydrazinoadenosine (WRC-0470): a novel, short-acting adenosine A_{2a} receptor agonist. Circulation 1996;94:1726–32.
19. Heyman MA, Payne BD, Hoffman JIE, Rudolph AM. Blood flow measurements with radionuclide-labeled particles. Prog Cardiovasc Dis 1977;20:55–79.
20. Utley J, Carlson EL, Hoffman JIE, Martinez HM, Buckberg GD. Total and regional myocardial blood flow measurements with 25μ, 15μ, 9μ, and filtered 1–10μ diameter microspheres and antipyrine in dogs and sheep. Circ Res 1974;34:391–405.
21. Falsetti HL, Carroll RJ, Marcus ML. Temporal heterogeneity of myocardial blood flow in anesthetized dogs. Circulation 1975;52:848–53.
22. Beppu S, Matsuda H, Shishido T, Matsumura M, Miyatake K. Prolonged myocardial contrast echocardiography via peripheral venous administration of QW3600 injection (Echo Gen®): its efficacy and side effects. J Am Soc Echocardiogr 1997;10:11–24.
23. Rouleau J, Boerboom LE, Surjadhana A, Hoffman JIE. The role of autoregulation and tissue diastolic pressures in the transmural distribution of left ventricular blood flow in anesthetized dogs. Circ Res 1979;45:804–15.
24. Gould KL, Lipscomb K. Effects on coronary stenoses on coronary flow reserve and resistance. Am J Cardiol 1974;34:48–55.
25. Jugdutt BI, Hutchins GM, Bulkley BH, Becker LC. Myocardial infarction in the conscious dog: three dimensional mapping of infarct, collateral flow, and region at risk. Circulation 1979;60:1141–50.
26. Gopal AS, Keller AM, Rigling R, King DL. Left ventricular volume and endocardial surface area by three-dimensional echocardiography: comparison with two-dimensional echocardiography and nuclear magnetic resonance imaging in normal subjects. J Am Coll Cardiol 1993;22:258–70.
27. Sapin PM, Clarke GB, Gopal AS, Smith MD, King DL. Validation of three-dimensional echocardiography for quantifying the extent of dyssynergy in canine acute myocardial infarction—comparison with two-dimensional echocardiography. J Am Coll Cardiol 1996;27:1761–70.
28. Germano G, Van Train KF, Garcia EV, et al. Quantitation of myocardial perfusion with SPECT: current issues and future trends. In: Zaret BL, Beller GA, editors. Nuclear Cardiology. State of the Art and Future Directions. St. Louis: CV Mosby, 1993:77–88.

29. Weisskoff RW. Principles and instrumentation for cardiac magnetic resonance imaging. In: Skorton DJ, Schelbert HR, Wolf GL, Brundage BH, editors. Marcus Cardiac Imaging: A Companion to Braunwald's Heart Disease. Philadelphia: Saunders, 1996:639–52.
30. Fleishman CE, Ota T, Lewis CW, et al. Quantitative assessment of LV ischemic risk volume using real-time three-dimensional echocardiography [abstract]. Circulation 1996;94 Suppl I:I-687.
31. Ito H, Tomooka T, Sakai N, et al. Lack of myocardial perfusion immediately after successful thrombolysis: a predictor of poor recovery of left ventricular function in anterior myocardial infarction. Circulation 1992; 85:1699–705.
32. Ragosta M, Camarano G, Kaul S, Powers ER, Sarembock IJ, Gimple LW. Microvascular integrity indicates myocellular viability in patients with recent myocardial infarction: new insights using myocardial contrast echocardiography. Circulation 1994;89:2562–9.
33. Lim YJ, Nanto S, Masuyama T, Kohama A, Hori M, Kamada T. Myocardial salvage: its assessment and prediction by the analysis of serial myocardial contrast echocardiograms in patients with acute myocardial infarction. Am Heart J 1994;128:649–56.
34. Sabia PJ, Powers ER, Jayaweera AR, Ragosta M, Kaul S. Functional significance of collateral blood flow in patients with recent acute myocardial infarction: a study using myocardial contrast echocardiography. Circulation 1992;85:2080–9.
35. Villanueva FS, Spotnitz WD, Jayaweera AR, Gimple LW, Dent J, Kaul S. On-line intra-operative quantitation of regional myocardial perfusion during coronary artery bypass graft operations with myocardial contrast two-dimensional echocardiography. J Thorac Cardiovasc Surg 1992;104:1524–31.
36. Bayfield M, Lindner JR, Kaul S, Ismail S, Goodman NC, Spotnitz WD. Deoxygenated blood minimizes adherence of sonicated albumin microbubbles during cardioplegic arrest and after blood reperfusion: experimental and clinical observations with myocardial contrast echocardiography. J Thorac Cardiovasc Surg 1997;113:1100–8.